

Bridging the Gap between Learning and Inference for Diffusion-Based Molecule Generation

Peidong Liu^a, Wenbo Zhang^b, Xue Zhe^a, Jiancheng Lv^a and Xianggen Liu^{a,*}

^aCollege of Computer Science, Sichuan University, Chengdu 610065, China

^bDepartment of Biomedical Engineering, Tsinghua University, Beijing 100084, China

ARTICLE INFO

Keywords:

generative model
diffusion model
exposure bias
3D molecule generation

ABSTRACT

The efficacy of diffusion models in generating a spectrum of data modalities, including images, text, and videos, has spurred inquiries into their utility in molecular generation, yielding significant advancements in the field. However, the molecular generation process with diffusion models involves multiple autoregressive steps over a finite time horizon, leading to exposure bias issues inherently. To address the exposure bias issue, we propose a training framework named GapDiff. The core idea of GapDiff is to utilize model-predicted conformations as ground truth probabilistically during training, aiming to mitigate the data distributional disparity between training and inference, thereby enhancing the affinity of generated molecules. We conduct experiments using a 3D molecular generation model on the CrossDocked2020 dataset, and the vina energy and diversity demonstrate the potency of our framework with superior affinity. GapDiff is available at <https://github.com/HUGHNew/gapdiff>.

1. Introduction

Drug discovery entails a comprehensive understanding of the molecular underpinnings of disease pathophysiology, followed by the identification and synthesis of chemical entities or biopharmaceuticals capable of selectively modulating the pertinent biological pathways (Sneader, 2005). Among the numerous traditional methods, screening from natural products and serendipitous discoveries are the most renowned. The discovery of penicillin and artemisinin (White, 1997), two antibiotics, relied on the former method, while the drug repurposing of sildenafil (Eardley et al., 2002) for the treatment of erectile dysfunction owed to the latter approach. Subsequently, new biology-based and computer-assisted methods have achieved encouraging results (Mandal et al., 2009; Rognan, 2007; Batool et al., 2019). For instance, rational drug design lowers the overall cost by targeting known protein pockets, and high-throughput screening (Mayr and Bojanic, 2009) enables faster identification of molecules with potential drug activity.

In recent years, with the advancement of deep learning and the growing interest in AI for science, numerous new deep learning methods have emerged in the realm of drug discovery to accomplish drug generation tasks. Early methods based on molecular string representations (Grisoni et al., 2020; Arús-Pous et al., 2019; Schoenmaker et al., 2023), 2D molecular images (Walters and Barzilay, 2020) and 2D graph representations (Lim et al., 2020; Jin et al., 2018) have made some progress. Nevertheless, these approaches cannot perceive the 3D structure of molecules, which is crucial for understanding their biological activity and interactions.

Later, researchers who pay more attention to structure-based drug design (SBDD) (Anderson, 2003) and molecular 3D structure obtain significant improvement with Deep Learning approaches. Tomohide Masuda (Ragoza et al., 2022a) used 3D convolutional networks to represent 3D molecular grids, but CNNs lack rotational equivariance, which means they cannot fully capture the properties of molecules. With the introduction and widespread application of equivariant networks like SE(3)-equivariant (Fuchs et al., 2020) and E(n)-equivariant (Satorras et al., 2021), new advancements have been made with diffusion models based on 3D equivariant networks (Liu et al., 2022; Peng et al., 2022; Guan et al., 2022; Xu et al., 2021). These models are able to more accurately represent molecular properties by maintaining equivariance to rotations and translations, improving performance in 3D molecular generation tasks. Nonetheless, general diffusion models require a large number of iteration steps (typically 1000), leading to error accumulation and exposure bias issues.

*Corresponding author

EMAIL(s): peidong_liu@stu.scu.edu.cn (P. Liu); zhangwb19@mails.tsinghua.edu.cn (W. Zhang); zacharyxz@stu.scu.edu.cn (X. Zhe); lvjiancheng@scu.edu.cn (J. Lv); liuxianggen@scu.edu.cn (X. Liu)

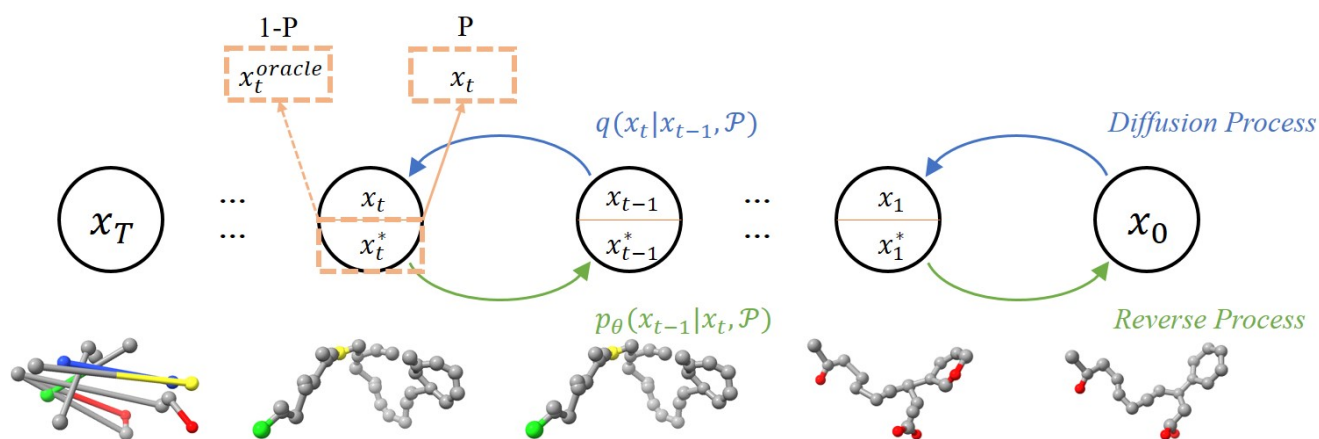


Figure 1: The overview of GapDiff pipeline with *oracle conformation*. Our diffusion process is consistent with the logic of DDPM, with the difference lying in the reverse process (the lower part indicated by the green arrow) during training. In the reverse process, the ground truth is selected probabilistically between the original ground truth (denoted as x_i like x_t) and the model's real-time predicted value (denoted as x_i^{oracle} like x_t^{oracle}), with a probability p_T favoring the original value. The starting point of the reverse process is a random conformation, such as x_T corresponding to a group of atoms with bonds, which serves as the initial random noise and cannot be reconstructed into a feasible molecule. In subsequent time steps, most of the noise is removed with the protein \mathcal{P} condition, and we can observe changes in the molecular conformation within the protein pocket. By the final steps, the conformation becomes mostly stable.

We observe that diffusion models share the same exposure bias issue as autoregressive models due to long-term autoregressive generation. This issue arises from the biased conditions during inference, which are not the ground truth in training. To address the exposure bias issue caused by data inconsistency, we propose an adaptive sampling strategy to estimate the real condition which can reduce the gap between training and sampling. To obtain the desired condition, we propose pseudo molecule estimation, whose core idea is to regard the model's current predictions as the ground truth instead of using the standard noisy sample in training time. Experiments on the CrossDocked2020 (Francoeur et al., 2020) dataset show that GapDiff generates molecules with better representation in 3D structure and protein binding affinity compared to the baseline.

Our main contributions can be summarized as follows:

- Considering the impact of exposure bias on 3D molecular generation, we propose an adaptive sampling strategy to address this issue, yielding promising results.
- We introduce the pseudo molecule estimation method and implement the adaptive sampling strategy, which incorporates model prediction noise into the training process based on theoretical grounds.
- Empirical results on CrossDocked2020 demonstrate the efficacy of our approach in molecule generation with higher affinity, achieving new SOTA docking scores.

2. Related Work

Molecule Generation. According to different representations, existing molecular generation models can be categorized into four major groups: string-based, image-based, 2D graph-based, and 3D structure-based methods. The most common molecular string representation is Simplified Molecular Input Line Entry System (SMILES) (Weininger, 1988), where many existing language models (such as RNN and Transformer) can be reused for molecular generation tasks (Grisoni et al., 2020; Arús-Pous et al., 2019; Schoenmaker et al., 2023; Brahmavar et al., 2024). 2D molecular image representations (Walters and Barzilay, 2020) and graph representations (Lim et al., 2020; Jin et al., 2018) employ CNNs and GNNs respectively for more information than string representations. However, they do not take into account the 3D structure and equivariant properties of molecules, so the generation quality is not as good as the 3D representation model (Liu et al., 2022; Peng et al., 2022; Guan et al., 2022; Xu et al., 2021; Guan et al., 2023; Huang et al., 2024).

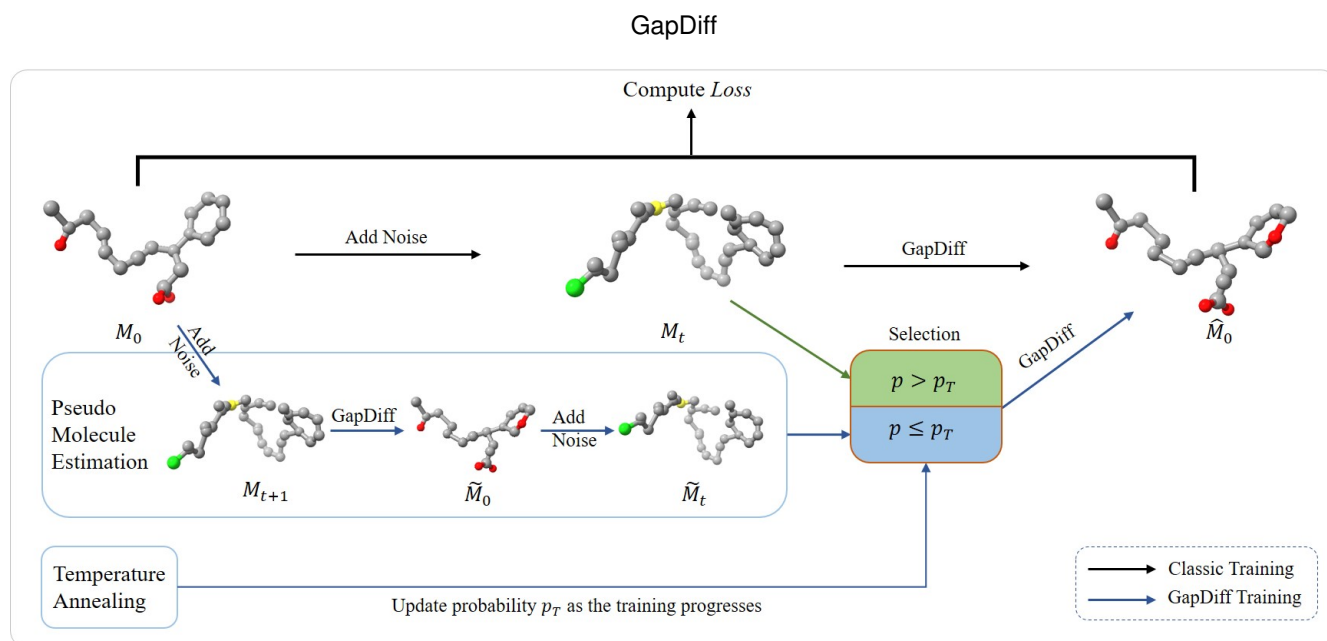


Figure 2: The proposed sampling strategy of GapDiff. We use arrows of different colors to distinguish between the classic method and ours.

Diffusion Models. DPM (Sohl-Dickstein et al., 2015) introduced diffusion models as a new family of generative models. After improved by (Ho et al., 2020; Song and Ermon, 2019; Song et al., 2021), diffusion models have been applied in various fields like unconditional image generation (Ho et al., 2020), text-to-image generation (Nichol et al., 2022), audio domain (Mittal et al., 2021), time series forecasting (Rasul et al., 2021) and other generative tasks (Croitoru et al., 2023). Recently, many researches have also applied Diffusion models to molecular generation, particularly in the field of Structure-Based Drug Design (SBDD) (Guan et al., 2022, 2023; Huang et al., 2024). For instance, TargetDiff (Guan et al., 2022) combined with an SE(3)-equivalent network, has surpassed the previous SOTA method, Pocket2Mol (Peng et al., 2022), with a significant docking score on the CrossDock2020 dataset. DecompDiff (Guan et al., 2023), which incorporates molecular properties, utilizes a diffusion model for fragment synthesis and bond diffusion, further demonstrating the effectiveness of diffusion models in molecular generation.

Exposure Bias. Deep learning inherently assumes that the data during training and testing are independent and identically distributed (IID). However, in practical applications, due to sampling biases and specific application constraints, this assumption is often difficult to satisfy, which gives rise to the issue of exposure bias (Chen et al., 2023). Although this issue has been extensively studied in the fields of recommendation algorithms and Natural Language Processing (NLP) (Yang et al., 2018; Lamb et al., 2016; Zhang et al., 2019), there is relatively less research on diffusion models in this regard. DDPM-IP (Ning et al., 2023) aims to alleviate the exposure bias issue by explicitly modeling the prediction error using a Gaussian input perturbation at training time. While ADM-ES (Ning et al., 2024) analytically models the sampling distribution and obtains further discussion on this topic.

3. Problem Definition

The problem of protein-based 3D molecular generation is defined as a conditional generation process under the specific protein pocket. Formally speaking, a data point consists of pairs of proteins \mathcal{P} and molecular conformations \mathcal{M} . The molecular conformation is represented by the concatenation of its atomic 3D Cartesian coordinates $x \in \mathcal{R}^{m \times 3}$ and one-hot encoded atomic types $v \in \mathcal{R}^{m \times k}$ (m denotes the length of the molecule and k shows the number of potential atomic types), and so is the protein. That is, the goal of GapDiff is to generate a reasonable molecular conformation $\mathcal{M} = [x, v]$ given the protein $\mathcal{P} = [x_p, v_p]$ using a novel diffusion model.

4. Methodology

4.1. Classic Diffusion Process

The diffusion model defines the *diffusion process* with the data $\mathbf{x}_0 \sim q(\mathbf{x}_0)$, which is a Markov chain that incrementally adds Gaussian noise in equation 1 using schedule hyperparameters β_1, \dots, β_T .

$$q(\mathbf{x}_{1:T}|\mathbf{x}_0) := \prod_{t=1}^T q(\mathbf{x}_t|\mathbf{x}_{t-1}), \quad q(\mathbf{x}_t|\mathbf{x}_{t-1}) := \mathcal{N}(\mathbf{x}_t; \sqrt{1 - \beta_t}\mathbf{x}_{t-1}, \beta_t\mathbf{I}) \quad (1)$$

Based on the properties of the Gaussian distribution, this process of incrementally adding noise $q(\mathbf{x}_t|\mathbf{x}_0)$ can be simplified in equation 2 with notations $\alpha_t := 1 - \beta_t$; $\bar{\alpha}_t := \prod_{s=1}^t \alpha_s$.

$$q(\mathbf{x}_t|\mathbf{x}_0) = \mathcal{N}(\mathbf{x}_t; \sqrt{\bar{\alpha}_t}\mathbf{x}_0, (1 - \bar{\alpha}_t)\mathbf{I}) \quad (2)$$

The diffusion model is a parameterized Markov chain that models a latent variable model of the form $p_\theta(\mathbf{x}_0) := \int p_\theta(\mathbf{x}_{0:T})d\mathbf{x}_{1:T}$, used to learn the reverse Gaussian denoising process of the diffusion process $p_\theta(\mathbf{x}_{t-1}|\mathbf{x}_t)$, i.e. the *reverse process*. And the *reverse process* can be formalized as a normal distribution in equation 3 because the forward process consists of thousands of steps and each one ($q(\mathbf{x}_t|\mathbf{x}_{t-1})$) follows a Gaussian distribution.

$$p_\theta(\mathbf{x}_{0:T}) := p(\mathbf{x}_T) \prod_{t=1}^T p_\theta(\mathbf{x}_{t-1}|\mathbf{x}_t), \quad p_\theta(\mathbf{x}_{t-1}|\mathbf{x}_t) := \mathcal{N}(\mathbf{x}_{t-1}; \mu_\theta(\mathbf{x}_t, t), \sum_{\theta}(\mathbf{x}_t, t)) \quad (3)$$

Intuitively, what we need to know is the denoising distribution $q(\mathbf{x}_{t-1}|\mathbf{x}_t)$ of the data, but it is not tractable. Instead, we can compute the forward process posteriors of the data $q(\mathbf{x}_{t-1}|\mathbf{x}_t, \mathbf{x}_0)$ in equation 4 applying Bayes theorem.

$$q(\mathbf{x}_{t-1}|\mathbf{x}_t, \mathbf{x}_0) = \mathcal{N}(x_{t-1}; \tilde{\mu}(\mathbf{x}_t, \mathbf{x}_0), \tilde{\beta}\mathbf{I}) \quad (4)$$

The objective of diffusion models is to narrow the divergence between the denoising Gaussian distribution (i.e. ground truth) $q(\mathbf{x}_{t-1}|\mathbf{x}_t, \mathbf{x}_0)$ and the predicted distribution $p_\theta(\mathbf{x}_{t-1}|\mathbf{x}_t)$, where the condition \mathbf{x}_t is sampled from the unbiased Gaussian distribution. That is, learn the data distribution by minimizing equation 5.

$$J = E \left[\sum_{t \geq 1} D_{\text{KL}}(q(\mathbf{x}_{t-1}|\mathbf{x}_t, \mathbf{x}_0) || p_\theta(\mathbf{x}_{t-1}|\mathbf{x}_t)) \right] \quad (5)$$

4.2. The GapDiff Framework

GapDiff adopts the diffusion process to learn the conformations M of a molecule in the 3D space. In GapDiff, the molecule state M_t at step t can be determined by the previous state M_{t-1} and the protein structure \mathcal{P} . $M_t = [x_t, v_t]$ is the molecule state at step t . To reduce the computational complexity, we assume the atom coordinates x_t and the identity v_t are independent in the estimation of the transformation probability $q(M_t|M_{t-1}, \mathcal{P})$.

$$q(M_t|M_{t-1}, \mathcal{P}) = P(x_t|x_{t-1}, \mathcal{P})P(v_t|v_{t-1}, \mathcal{P}) \quad (6)$$

We model the transformation probability of atomic positions $P(x_t|x_{t-1}, \mathcal{P})$ and that of the atomic types $P(v_t|v_{t-1}, \mathcal{P})$ using a normal distribution and a categorical distribution (K represents the number of categories), respectively. The forward details are shown in algorithm 1.

$$P(x_t|x_{t-1}, \mathcal{P}) = \mathcal{N}(x_t; \sqrt{1 - \beta_t}x_{t-1}, \beta_t\mathbf{I}|\mathcal{P}), \quad P(v_t|v_{t-1}, \mathcal{P}) = C(v_t|(1 - \beta_t)v_{t-1} + \beta_t/K, \mathcal{P}) \quad (7)$$

As for the inference of GapDiff, it starts with noises M_T and iteratively denoises from the previous result, finally achieving the goal. That is,

$$p_\theta(M_{0:T}) := p(M_T) \prod_{t=1}^T p_\theta(M_{t-1}|M_t), \quad M_t \sim p_\theta(M_t|M_{t+1}) \quad (8)$$

where the condition of the denoising process is generated in the last step $p_\theta(M_{t-1}|M_t)$, instead of the sample from the unbiased Gaussian distribution.

Algorithm 1 Forward Process

Require: original conformation M_0 , timestep t .

- 1: We compute $M_t = [x_t, v_t]$ in two parts: atomic positions x_t and atomic types v_t
- 2: $x_t = \sqrt{\bar{\alpha}_t}x_0 + \sqrt{(1 - \bar{\alpha}_t)}\epsilon$, where $\epsilon \sim \mathcal{N}(1, 0)$
- 3: $v_t = \text{one_hot}(\text{argmax}[\log(\bar{\alpha}_t v_0 + (1 - \bar{\alpha}_t)/K) + g])$, where $g \sim \mathbf{Gumble}(0, 1)$

Exposure bias. The discrepancy between training and inference is referred to the exposure bias problem, which may lead to an accumulation of errors and distortion of generation. Especially in 3D molecule generation, the conformation space of 3D molecules is huge and rough, with most breaking the chemical and physical rules. A small position shift could result in an unreal conformation or lower affinity. During inference, the reverse process can be viewed as an autoregressive generative process iterated multiple times in time steps, generating M_0 by gradually denoising M_t sampled randomly according to equation 3. However, general diffusion models require a large number of iteration steps (typically 1000), leading to error accumulation and exposure bias issues.

Adaptive Sampling Strategy. To address the exposure bias issue in traditional diffusion models, we propose an adaptive sampling strategy, which reduces the discrepancy in data distribution between training and inference by introducing reasonable noise into the training phase. The core idea of GapDiff is to probabilistically utilize model-predicted conformations as ground truth during training. Temporarily disregarding condition protein \mathcal{P} , we denote y_t as the first term in the condition of the denoising probability $q(M_{t-1}|M_t, M_0)$, an estimated conformation based on M_t and t in equation 9 (right). That is, we use the estimated conformation y_t to predict the denoised sample M_{t-1} and update the objective function in equation 9 (left).

$$E \left[\sum_{t \geq 1} D_{\text{KL}}(q(M_{t-1}|y_t, M_0) || p_{\theta}(M_{t-1}|y_t)) \right], \quad y_t = \text{Estimation}(M_t, t) \quad (9)$$

GapDiff’s sampling strategy in Figure 2 shows how we eliminate the gap between training and inference. The black arrow indicates the classic way while the blue line represents our modified training process. We utilize two procedures to boost the whole training process. The first one, called pseudo molecule estimation, gives an estimate of the current time step for single-step denoising. Meanwhile, the temperature annealing algorithm updates the critical probability p_T as the training progresses. Then we select the denoising result of the previous step or the new estimate with a certain probability to make the model closer to the data distribution of inference during training.

Pseudo Molecule Estimation. To estimate the *oracle conformation* as the desired condition, we propose pseudo molecule estimation, whose core idea is to regard the model’s current predictions as the ground truth instead of using the standard noisy sample in training time (details in algorithm 2). Using this estimate allows the model to make the data distribution during training a weighted average of the true distribution and the model’s learned distribution. This reduces the gap between training and inference.

As GapDiff predicts the original conformation (i.e. M_0), we can obtain the prediction \hat{M}_0 directly and estimate the oracle conformation \hat{M}_t . Following the core idea, we compute the next timestep status of molecule $M_{t+1} = [x_{t+1}, v_{t+1}]$ by algorithm 1. Then, we predict \hat{M}_0 with GapDiff under the noisy conformation M_{t+1} and protein \mathcal{P} . Finally, we obtain the oracle conformation \hat{M}_t through the diffusion process same as the way we get M_{t+1} .

$$\hat{x}_0 = \phi(x_{t+1}, t + 1, \mathcal{P}) \quad (10)$$

Theoretically, we can select any time step’s noisy conformation to predict the original conformation and use this to compute the *oracle conformation*. To better simulate the inference environment during prediction, we choose the previous time step to predict the value at the current time step t . Specifically, we calculate the current state from the state at time step $t + 1$. This prediction method more closely mirrors the inference process compared to other time-step selections. Additionally, making single-step predictions is a trade-off considering time costs and boundary conditions. When the randomly sampled time step is $t = T$, we do not compute the *oracle conformation*.

We define $y_{x_t} = f(x_t, \hat{x}_t)$, denoted as positions of the pseudo molecule, and y_{x_t} is a estimation between x_t and \hat{x}_t which picks x_t with probability p (equation 11, that is the probability over the critical probability p_T). We compute y_{v_t} applying the same way.

$$P(y_t) = \begin{cases} p, & y_{xt} = x_t, y_{vt} = v_t \\ 1 - p, & y_{xt} = \hat{x}_t, y_{vt} = \hat{v}_t \end{cases} \quad (11)$$

Algorithm 2 Pseudo Molecule Estimation

Require: Protein-ligand binding $\{\mathcal{P}, \mathcal{M} = [x_0, v_0]\}$, current timestep t .

- 1: Perturb x_0, v_0 to obtain x_{t+1}, v_{t+1} according to algorithm 1.
 - 2: Predict \hat{x}'_0, \hat{v}'_0 from x_{t+1}, v_{t+1} with $\phi_\theta(x_{t+1}, v_{t+1}, t + 1, \mathcal{P})$.
 - 3: Perturb \hat{x}'_0, \hat{v}'_0 to obtain \hat{x}_t, \hat{v}_t same as step 1.
 - 4: Obtain pseudo molecule $\tilde{M}_t = [y_{xt}, y_{vt}]$ giving with probability p using equation 11.
-

Probability Temperature Annealing. Hoping the model can learn the data distribution more smoothly during training, We use monotonic decline functions to control the selection probability. Intuitively, we need this probability curve to have a lower cooling rate at the beginning of training, that is, a smaller derivative value, and a higher cooling rate at the end of training, so that it can quickly adapt to changes from training to inference. We take the OR (Zhang et al., 2019) model's curve as the first one, which goes with a hyperparameter (equation 12) and is borrowed from Bengio (Bengio et al., 2015). However, under its default setting (shown in Setup), the probability p_T cools too quickly, which is not conducive to learning a robust data distribution.

$$p_T = \frac{\mu}{\mu + \exp(e/\mu)} \quad (12)$$

So we propose two other temperature anneals, one is linear annealing (equation 13) and the other is arc annealing (equation 14). For the sake of conciseness, this can also be regarded as $p = \sqrt{r^2 - e^2}/r$, we use a modified quarter circle curve as the cooling curve, make the result a real number and finally regularize it to ensure that the curve value range is in $[0, 1]$. In order to avoid p_T being too low in the later stages of training, the model basically enters the self-verification learning stage, which has been reinforcing bias and making it difficult to learn the original distribution. We use $\min(p, \text{lower_bound})$ to obtain the probability of actual use.

$$p_T = 1 + \text{slope} * e \quad (13)$$

$$p_T = \sqrt{\max(r^2 - (e/100)^2, 0)}/r \quad (14)$$

Algorithm 3 Training Procedure

Require: Protein-ligand binding dataset $\{\mathcal{P}, \mathcal{M}\}_{i=1}^N$, neural network ϕ_θ .

- 1: **while** ϕ_θ not converge **do**
 - 2: Sample timestep $t \in \mathcal{U}(0, \dots, T)$.
 - 3: Move the complex to make CoM (Center of Mass) of protein atoms zero.
 - 4: Perturb $M_0 = [x_0, v_0]$ to obtain $M_t = [x_t, v_t]$ using algorithm 1 in forward process.
 - 5: Obtain pseudo molecule estimation $\tilde{M}_t = [y_{xt}, y_{vt}]$ with $\text{PME}(x_t, v_t, t, p, \mathcal{P})$ using algorithm 2.
 - 6: Predict $\hat{M}_0 = [\hat{x}_0, \hat{v}_0]$ from $\tilde{M}_t = [y_{xt}, y_{vt}]$ with $\phi_\theta: \phi_\theta(y_{xt}, y_{vt}, t, \mathcal{P})$.
 - 7: Compute the posterior atom types $c(y_{vt}, v_0)$ and $c(y_{vt}, \hat{v}_0)$ according to equation 9,10 in the appendix B.
 - 8: Compute the unweighted MSE loss on atom coordinates and the KL loss on posterior atom types: $L = ||x_0 - \hat{x}_0||^2 + \alpha \text{KL}(c(y_{vt}, v_0) || c(y_{vt}, \hat{v}_0))$.
 - 9: Update θ by minimizing L .
 - 10: **end while**
-

Overview of GapDiff. The complete training process is detailed in algorithm 3, and the pipeline is shown in Figure 2. First, we sample a time step t from a uniform distribution \mathcal{U} (line 2) and set the protein centroid as the origin of the

Table 1

Summary of different properties of reference molecules and molecules generated by our model and other baselines. We compared our models (TargetDiff+Ours, BindDM+Ours) sequentially with all other models, indicating the best performing method in each case in **bold** and highlighting the metrics where our method achieved second place with underlining. In the subsequent text, we will use GAPDIFF to represent BindDM+Ours.

Metrics	Vina Score(↓)		Vina Min(↓)		Vina Dock(↓)		High Affinity(↑)		QED(↑)		SA(↑)		Diversity(↑)	
	Avg.	Med.	Avg.	Med.	Avg.	Med.	Avg.	Med.	Avg.	Med.	Avg.	Med.	Avg.	Med.
Reference	-6.36	-6.46	6.71	-6.49	-7.45	-7.26	-	-	0.48	0.47	0.73	0.74	-	-
liGAN	-	-	-	-	-6.33	-6.20	21.1%	11.1%	0.39	0.39	0.59	0.57	0.66	0.67
GraphBP	-	-	-	-	-4.80	-4.70	14.2%	6.7%	0.43	0.45	0.49	0.48	0.79	0.78
AR	-5.75	-5.64	-6.18	-5.88	-6.75	-6.62	37.9%	31.0%	0.51	0.50	0.63	0.63	0.70	0.70
Pocket2Mol	-5.14	-4.70	-6.42	-5.82	-7.15	-6.79	48.4%	51.1%	0.56	0.57	0.74	0.75	0.69	0.71
DecompDiff	-5.67	-6.04	-7.04	-7.09	-8.39	<u>-8.43</u>	64.4%	71.0%	0.45	0.43	0.61	0.60	0.68	0.68
TargetDiff	-5.47	-6.30	-6.64	-6.83	-7.80	-7.91	58.1%	59.1%	0.48	0.48	0.58	0.58	0.72	0.71
TargetDiff+Ours	-6.51	-7.18	-7.50	-7.38	-8.54	-8.38	<u>59.0%</u>	<u>62.8%</u>	0.46	0.46	0.56	0.56	0.79	<u>0.77</u>
BindDM	-5.92	-6.81	-7.29	-7.34	-8.41	-8.37	64.8%	71.6%	0.51	0.52	0.58	0.58	0.75	0.74
BindDM+Ours	-6.28	-6.90	-7.39	-7.45	-8.43	-8.47	68.9%	72.2%	<u>0.51</u>	<u>0.52</u>	0.59	0.58	0.75	0.75

coordinates (line 3). Then, we sequentially add noise to the atomic coordinates and atomic types according to the diffusion process equations which are represented in algorithm 1 (line 4). For the atomic 3D coordinates, we add noise from a normal distribution; for the atomic types, we discretize them and add Gumbel noise. Based on the noisy molecular information $M_t = [x_t, v_t]$, the time step t , and the protein information \mathcal{P} , we obtain a molecular estimate, i.e. *oracle molecule*, with a certain probability p (line 5). In practice, we let the neural network output the predicted original molecule (line 6) and then compute the loss by comparing it to the original molecule, calculating the distance for coordinates and the divergence for type distributions (lines 7-9). This loss is used to perform backpropagation to update the neural network until convergence (lines 1 & 10).

5. Experiments

5.1. Setup

Data. We use CrossDocked2020 (Francoeur et al., 2020), the commonly used protein-ligand pairs dataset, as a benchmark dataset for both training and evaluation. Similar to (Luo et al., 2021; Guan et al., 2022, 2023; Huang et al., 2024), we filter the complexes with RMSD (Root Mean Square Deviation, the measure of the average distance between the atoms of superimposed molecules) higher than 1 Å and remains 100,000 pairs for training, 100 pairs for testing.

Baseline. We use our model to compare the affinity of the generated molecules with liGAN (Ragoza et al., 2022b), AR (Luo et al., 2021), Pocket2Mol (Peng et al., 2022), GraphBP (Liu et al., 2022), TargetDiff (Guan et al., 2022), DecompDiff (Guan et al., 2023) and BindDM (Huang et al., 2024). In particular, TargetDiff, DecompDiff, and BindDM represent previous state-of-the-art performance in 3D molecule generation to a given protein structure with diffusion process and equivariant graph neural network, considering rotational and translational equivariance.

GapDiff. We employ the E(n)-Equivariant GNN (Satorras et al., 2021) as the backbone model which contains 9 equivariant layers and make diffusion steps $T = 1000$ the same as DDPM. As liGAN and AR do, we choose OpenBabel (O’Boyle et al., 2011) to reconstruct the 3D molecule from atom coordinates. We use the Adam optimizer, with $\beta = (0.95, 0.999)$ and a learning rate of 1e-4, without weight decay. Following the settings of TargetDiff, we set the max training step to 200K and the batch size to 4 for all the models we have trained. In the scenario, the probability of not computing the prediction $P(t = T - 1)^{\text{batchsize}}$ is 0.996, which is acceptable and can be ignored. During training, we define the pseudo-epoch for probability update: epoch = step/1000, the initial value of p_T is 1, and the global seed is 2021. The temperature annealing function is arc annealing (equation 14), where $r = 2$ and the index of training epochs e starts from 0. By the way, we use $\mu = 12$ and slope = -0.005 for the original and linear curves as the default settings respectively. More details can be viewed in the configuration file after code released. The pipeline of training, sampling, and evaluation is driven on Ubuntu 20.04 with AMD EPYC 7542 Processor and NVIDIA GeForce RTX

GapDiff

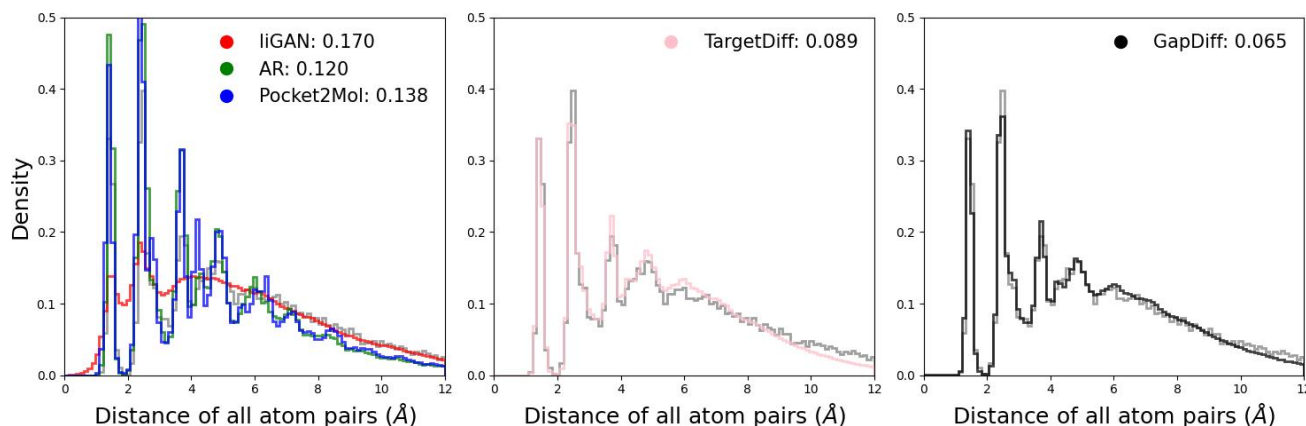


Figure 3: Comparing the distribution for distances of all-atom for reference molecules in the test set (gray) and generated molecules (color). Jensen-Shannon divergence (JSD \downarrow) between two distributions is reported.

Table 2

Jensen-Shannon divergence between the bond distance for reference and the generated. And we highlight the best 3 results with **bold text**, underlined text, and *italic text* respectively.

Bond(\downarrow)	liGAN	AR	Pocket2Mol	TargetDiff	DecompDiff	BindDM	GAPDIFF
C-C	0.601	0.609	0.496	<i>0.369</i>	<u>0.359</u>	0.380	0.357
C-N	0.634	0.474	0.416	0.363	<u>0.344</u>	<u>0.265</u>	0.253
C-O	0.656	0.492	0.454	0.421	<u>0.376</u>	0.329	<i>0.388</i>
C=C	0.665	0.620	0.561	<i>0.505</i>	<u>0.537</u>	<u>0.229</u>	0.189
C=N	0.749	0.635	0.629	<i>0.550</i>	0.584	0.245	<u>0.260</u>
C=O	0.661	0.558	0.516	0.461	<u>0.374</u>	0.249	<u>0.376</u>
C:C	0.497	0.451	0.416	<i>0.263</i>	<u>0.251</u>	0.282	0.141
C:N	0.638	0.552	0.487	<u>0.235</u>	<u>0.269</u>	0.130	<i>0.240</i>

3090. The virtual environment was created by micromamba with Python 3.9, the latest version under the package environment constraints. While NVIDIA driver version used is 525.125.06. Additional details regarding the software environment and installation procedures can be found in the README file within the code repository.

5.2. Results

We conduct several experiments to compare our method against the aforementioned baseline models, primarily evaluating the performance of our approach in terms of the quality of generated molecules. The main data are presented in four aspects: chemical bond distributions, binding affinity, molecular properties, and the versatility of GapDiff. Additionally, we perform ablation experiments to verify the rationale behind the hyperparameter selection of the adaptive sampling strategy.

Bond Distribution. First, we consider the distribution of atomic coordinates and the most common types of bonds connected to carbon atoms after applying the adaptive sampling strategy. In particular, the bond types include carbon-carbon bonds, carbon-nitrogen bonds, and carbon-oxygen bonds, covering single bonds(‘-’), double bonds(‘=’), and aromatic bonds(‘.’). We evaluate the difference between the generated bonds and the reference bonds using the Jensen-Shannon divergence (Lin, 1991), where a lower value indicates better performance.

As shown in Table 2, the molecules generated by our method are among the best three results, comparable to BindDM and surpassing other models. Meanwhile, our approach exhibits a significant advantage across all carbon bonds, particularly in double and aromatic bonds, where the latter achieves a twofold improvement over the previous best result. We see in Figure 3 that GAPDIFF achieves the lowest JSD of 0.065 to reference in all-atom pairs distance distribution of the ligands in test sets, exceeding notably TargetDiff and others. That is to say, the molecules generated by GAPDIFF surpass those produced by prior methods overall.

GapDiff

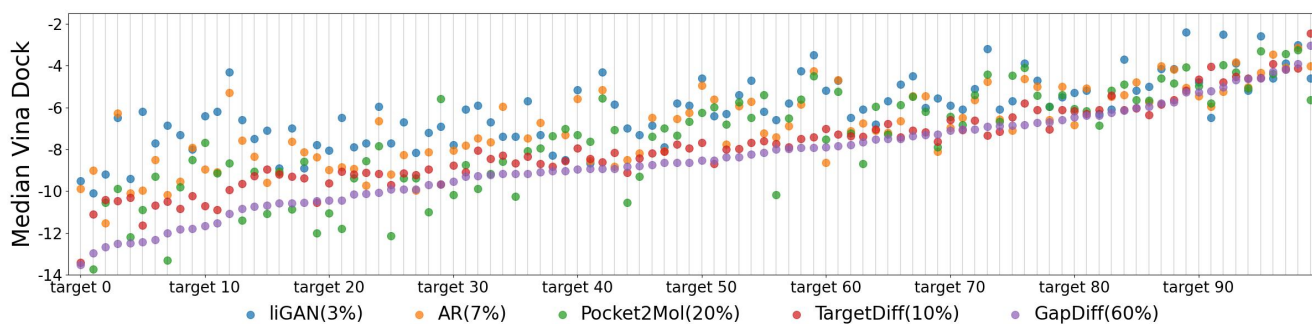


Figure 4: Median Vina Dock energy for five models across 100 testing targets. The percentage represents the proportion of the model achieving the best binding affinity on the test set.

Binding Affinity. The binding affinity between a molecule and a protein is measured by the energy released after binding. AutoDock Vina (Eberhardt et al., 2021) is usually used to calculate the energy, which acts as a crucial evaluation metric. Therefore, we take the docking scores and the results compared with the reference as metrics to compare and evaluate all the models which are Vina Score, Vina Min, Vina Dock, and High Affinity respectively. Vina Score is used to evaluate the stability of the small molecule-protein binding, Vina Min represents the minimum value during the docking process, Vina Dock energy attempts to find the lowest energy binding conformation and High Affinity exhibits the proportion of superiority over the reference on Vina Dock. As indicated in Table 1, GAPDIFF obtains higher mean and median in all affinity-related metrics compared to the baselines with the highest improvement reaching 4.1% in the mean of High Affinity. Otherwise, we reorder the median Vina Dock in ascending order according to our method for five methods. The results in Figure 4 show that our method outperforms all other methods in 60% of cases, which is more than all others combined.

Molecular Properties. As for property-related metrics, drug-likeness QED (Bickerton et al., 2012), synthesizability SA (Ertl and Schuffenhauer, 2009) and diversity are commonly used for evaluation. Unlike that DecompDiff accepts a trade-off between property-related metrics and affinity-related metrics, we maintain proper properties and make somewhat progress in the mean of SA and the median of diversity in Table 1. Nevertheless, we put less attention on QED and SA because many invalid molecules will be filtered out by virtual screening and it would be acceptable in a reasonable range.

Framework Versatility. Initially, we utilized the model architecture of TargetDiff for testing the GapDiff framework due to its simplicity, resulting in the TargetDiff+Ours variant. This variant achieves an average improvement of 0.89 in the mean of docking scores while maintaining a minimal decrease in the properties of QED and SA. Additionally, it delivers an approximate 9% enhancement in diversity which is comparable to GraphBP. Then, we conduct experiments on DecompDiff and BindDM, which share the same issue with TargetDiff, with the same hyper-parameters as TargetDiff+Ours. And we obtain BindDM+Ours which is regarded as GAPDIFF and discussed above. Meanwhile, we failed to fit DecompDiff due to reconstructing failure on all molecules during training and reproducing them. As the GapDiff framework has successfully applied to two diffusion models, we confirm that it would be a great plug-in framework for diffusion models to boost performance overall.

5.3. Ablation Study

These are two ablation studies to validate the rationality of our method. The first study focuses on the selection of annealing strategies, while the second involves the specific parameter settings of the selected annealing method.

Choice of Annealing Strategy. We employ ablation experiments for comparison to filter out the best method which considered the impact of both the lower bound and the annealing method. Due to the time-consuming nature of sampling and evaluating the full test dataset of 100 targets, we randomly selected 10 targets for the ablation experiments and used the docking scores as the evaluation metrics.

GapDiff

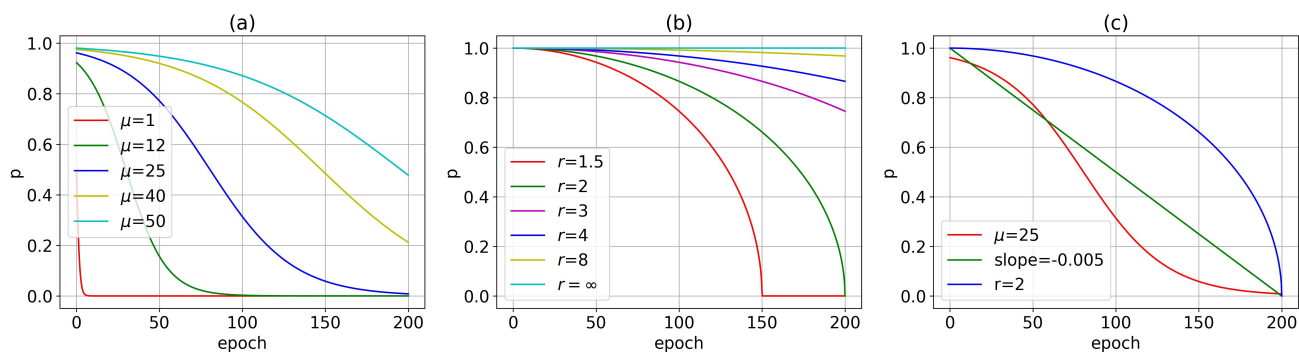


Figure 5: (a) is the original annealing comparison. (b) is the arc annealing comparison. And (c) is the comparison of the curves.

Table 3

Annealing methods comparison across 10 testing targets.

Metrics \ Annealing	Lower Bound	Vina Score(↓)		Vina Min(↓)		Vina Dock(↓)		
		Avg.	Med.	Avg.	Med.	Avg.	Med.	Avg.
Original (equation 12)	0.5	-4.588	-4.705	-4.898	-4.893	-5.661	-5.540	-5.047
	0.8	-4.209	-4.343	-4.544	-4.580	-5.471	-5.392	-4.757
Linear (equation 13)	0.5	-6.564	-6.499	-6.617	-6.241	-7.421	-7.249	-6.765
	0.8	-6.662	-6.418	-6.593	-6.223	-7.317	-7.146	-6.727
Arc (equation 14)	0.5	-6.496	-6.384	-6.780	-6.525	-7.470	-7.369	-6.837
	0.8	-6.413	-6.189	-6.719	-6.445	-7.463	-7.398	-6.771

For the lower bound, we empirically select two values, 0.5 and 0.8. 0.5 is an intermediate value, which ensures that the selection rate of the estimation molecule in the final stage is the same as the noisy molecule. On the other hand, 0.8 is a slightly larger value, leaning more towards the classic diffusion process.

In terms of the annealing curve, we discover that arc annealing outperformed linear annealing in both Vina Min and Vina Dock, although it was slightly worse in the Vina Score. Overall, arc annealing outperformed the others at both lower bounds of 0.5 and 0.8, with it performing best when the lower bound was set to 0.5 in Table 3. Consequently, we ultimately choose arc annealing and set the lower bound to 0.5.

To visually demonstrate the probability update of different annealing curves, we have plotted three figures to separately illustrate the OR schedule, the arc annealing curve under different hyperparameters, and a comparison of the three curves in Figure 5.

We show the original annealing curves ($p = \mu / (\mu + \exp(e/\mu))$) first and it represents the curves when μ equals 1, 12, 25, 40, and 50. It can be observed that when μ is relatively small (less than or equal to 12), the probability p decreases rapidly, reaching a relatively low value of about 0.2 by the quarter of the training process (approximately 50 epochs). This rapid decrease may lead to the model prematurely biasing towards the distribution at inference time without fully learning the data distribution, thereby affecting the quality of the generated molecules. Simultaneously, as μ increases, the probability value remains relatively high (greater than 0.5) for a longer duration of the training period. For instance, the curve with μ equal to 50 maintains a value close to 0.5 until the end of training.

We plot the arc annealing with the hyper-parameter r vary from 1.5 to infinity which is formulated as $p = \sqrt{\max(r^2 - (e/100)^2, 0)}/r$ in equation 14. When r is large, the value of the curve will be large and will not change much during the training process. When r equals 2, the curve forms a complete quarter circle, which aligns with our previous intuitive expectation for the concave function of probability p_T . As r decreases, the probability p_T reaches zero earlier; conversely, as r increases, the curve approaches the line of $p = 1$. Both of these scenarios present issues similar to those observed in the OR schedule curve.

Finally, we incorporate linear annealing and directly compare the three annealing curves. Taking into account the previously mentioned tendency of the OR and arc schedules to rapidly shift towards the extremes when their values are too large or too small, we select the curve with $\mu = 25$, $r = 2$ and slope = -0.005 as the representative to make

Table 4
Annealing comparison for better hyper-parameter.

Model	Metrics		Vina Score(↓)		Vina Min(↓)		Vina Dock(↓)	
	Avg.	Med.	Avg.	Med.	Avg.	Med.	Avg.	Med.
$r=\infty$	-5.41	-6.01	-6.32	-6.28	-7.28	-7.39		
$r=8$	-5.55	-6.27	-6.49	-6.54	-7.35	-7.51		
$r=4$	-5.58	-6.10	-6.49	-6.54	-7.35	-7.51		
$r=3$	-5.61	-6.27	-6.49	-6.48	-7.53	-7.53		
$r=2$	-6.51	-7.18	-7.50	-7.38	-8.54	-8.38		
$r=1.5$	-5.63	-6.12	-6.41	-6.37	-7.32	-7.42		

the comparison. Overall, the arc curve better meets our expectation of slow initial changes followed by rapid decline in the later stages.

Arc Annealing Comparison. We initially hypothesized that the arc annealing curve would yield the best results when $r = 2$, although it remains to be validated. Therefore, we design a series of ablation experiments, selecting the values 1.5, 2, 3, 4, 8, and infinity to empirically determine the optimal value for the hyperparameter r . The experimental outcomes confirm our initial hypothesis.

When r equals infinity, p_T is 1, which corresponds to not using our method at all, resulting in the lowest Vina scores, thereby proving the effectiveness of our method. When r is set to 1.5, 3, 4, or 8, the results are comparable, indicating that even with the early introduction of estimation or fewer opportunities for estimation, there is still a certain degree of improvement. When r equals 2, the best results are achieved, surpassing TargetDiff.

6. Conclusion

This paper combines the adaptive sampling strategy with probabilistic temperature annealing to solve the problem of poor performance caused by the data inconsistency between the generated distribution and the original distribution of the diffusion models when generating molecules. When this method is applied to training, it only requires minor changes to achieve great enhancement. Besides, it seems to be versatile for diffusion models and needs further experiments to be verified as a common solution for all models.

7. Acknowledgements

This work was partly supported by the National Natural Science Foundation of China under Grant (62206192) and the Natural Science Foundation of Sichuan Province under Grant (2023NSFSC1408).

CRedit authorship contribution statement

Peidong Liu: He has refined the theoretical framework of this study, conducted ablation experiments for the selection of annealing curves, and reported the experimental results on the TargetDiff and BindDM platforms (denoted as TargetDiff+Ours and BindDM+Ours).. **Wenbo Zhang:** He was responsible for the polishing and review of the manuscript.. **Xue Zhe:** He conducted the experiments on DecompDiff and obtained the findings.. **Jiancheng Lv:** He provided guidance, support and valuable comments during the planning and execution phases of the experiment.. **Xianggen Liu:** He proposed the research approach and guided the study..

References

- Anderson, A.C., 2003. The process of structure-based drug design. *Chemistry & biology* 10, 787–797.
- Arús-Pous, J., Johansson, S.V., Prykhodko, O., Bjerrum, E.J., Tyrchan, C., Reymond, J.L., Chen, H., Engkvist, O., 2019. Randomized smiles strings improve the quality of molecular generative models. *Journal of cheminformatics* 11, 1–13.
- Batool, M., Ahmad, B., Choi, S., 2019. A structure-based drug discovery paradigm. *International journal of molecular sciences* 20, 2783.
- Bengio, S., Vinyals, O., Jaitly, N., Shazeer, N., 2015. Scheduled sampling for sequence prediction with recurrent neural networks. *Advances in neural information processing systems* 28.

- Bickerton, G.R., Paolini, G.V., Besnard, J., Muresan, S., Hopkins, A.L., 2012. Quantifying the chemical beauty of drugs. *Nature chemistry* 4, 90–98.
- Brahmavar, S.B., Srinivasan, A., Dash, T., Krishnan, S.R., Vig, L., Roy, A., Aduri, R., 2024. Generating novel leads for drug discovery using llms with logical feedback, in: *Proceedings of the AAAI Conference on Artificial Intelligence*, pp. 21–29.
- Chen, J., Dong, H., Wang, X., Feng, F., Wang, M., He, X., 2023. Bias and debias in recommender system: A survey and future directions. *ACM Transactions on Information Systems* 41, 1–39.
- Croitoru, F.A., Hondru, V., Ionescu, R.T., Shah, M., 2023. Diffusion models in vision: A survey. *IEEE Transactions on Pattern Analysis and Machine Intelligence*.
- Eardley, I., Ellis, P., Boolell, M., Wulff, M., 2002. Onset and duration of action of sildenafil for the treatment of erectile dysfunction. *British journal of clinical pharmacology* 53, 61S–65S.
- Eberhardt, J., Santos-Martins, D., Tillack, A.F., Forli, S., 2021. Autodock vina 1.2. 0: New docking methods, expanded force field, and python bindings. *Journal of chemical information and modeling* 61, 3891–3898.
- Ertl, P., Schuffenhauer, A., 2009. Estimation of synthetic accessibility score of drug-like molecules based on molecular complexity and fragment contributions. *Journal of cheminformatics* 1, 1–11.
- Francoeur, P.G., Masuda, T., Sunseri, J., Jia, A., Iovanisci, R.B., Snyder, I., Koes, D.R., 2020. Three-dimensional convolutional neural networks and a cross-docked data set for structure-based drug design. *Journal of chemical information and modeling* 60, 4200–4215.
- Fuchs, F., Worrall, D., Fischer, V., Welling, M., 2020. Se (3)-transformers: 3d roto-translation equivariant attention networks. *Advances in neural information processing systems* 33, 1970–1981.
- Grisoni, F., Moret, M., Lingwood, R., Schneider, G., 2020. Bidirectional molecule generation with recurrent neural networks. *Journal of chemical information and modeling* 60, 1175–1183.
- Guan, J., Qian, W.W., Peng, X., Su, Y., Peng, J., Ma, J., 2022. 3d equivariant diffusion for target-aware molecule generation and affinity prediction, in: *The Eleventh International Conference on Learning Representations*.
- Guan, J., Zhou, X., Yang, Y., Bao, Y., Peng, J., Ma, J., Liu, Q., Wang, L., Gu, Q., 2023. Decomdiff: Diffusion models with decomposed priors for structure-based drug design, in: *International Conference on Machine Learning*, PMLR. pp. 11827–11846.
- Ho, J., Jain, A., Abbeel, P., 2020. Denoising diffusion probabilistic models. *Advances in neural information processing systems* 33, 6840–6851.
- Huang, Z., Yang, L., Zhang, Z., Zhou, X., Bao, Y., Zheng, X., Yang, Y., Wang, Y., Yang, W., 2024. Binding-adaptive diffusion models for structure-based drug design, in: *Proceedings of the AAAI Conference on Artificial Intelligence*, pp. 12671–12679.
- Jin, W., Barzilay, R., Jaakkola, T., 2018. Junction tree variational autoencoder for molecular graph generation, in: *International conference on machine learning*, PMLR. pp. 2323–2332.
- Lamb, A.M., ALIAS PARTH GOYAL, A.G., Zhang, Y., Zhang, S., Courville, A.C., Bengio, Y., 2016. Professor forcing: A new algorithm for training recurrent networks. *Advances in neural information processing systems* 29.
- Lim, J., Hwang, S.Y., Moon, S., Kim, S., Kim, W.Y., 2020. Scaffold-based molecular design with a graph generative model. *Chemical science* 11, 1153–1164.
- Lin, J., 1991. Divergence measures based on the shannon entropy. *IEEE Transactions on Information theory* 37, 145–151.
- Liu, M., Luo, Y., Uchino, K., Maruhashi, K., Ji, S., 2022. Generating 3d molecules for target protein binding, in: *International Conference on Machine Learning*, PMLR. pp. 13912–13924.
- Luo, S., Guan, J., Ma, J., Peng, J., 2021. A 3d generative model for structure-based drug design. *Advances in Neural Information Processing Systems* 34, 6229–6239.
- Mandal, S., Mandal, S.K., et al., 2009. Rational drug design. *European journal of pharmacology* 625, 90–100.
- Mayr, L.M., Bojanic, D., 2009. Novel trends in high-throughput screening. *Current opinion in pharmacology* 9, 580–588.
- Mittal, G., Engel, J.H., Hawthorne, C., Simon, I., 2021. Symbolic music generation with diffusion models, in: Lee, J.H., Lerch, A., Duan, Z., Nam, J., Rao, P., van Kranenburg, P., Srinivasamurthy, A. (Eds.), *Proceedings of the 22nd International Society for Music Information Retrieval Conference, ISMIR 2021, Online, November 7-12, 2021*, pp. 468–475. URL: <https://archives.ismir.net/ismir2021/paper/000058.pdf>.
- Nichol, A.Q., Dhariwal, P., Ramesh, A., Shyam, P., Mishkin, P., Mcgrew, B., Sutskever, I., Chen, M., 2022. Glide: Towards photorealistic image generation and editing with text-guided diffusion models, in: *International Conference on Machine Learning*, PMLR. pp. 16784–16804.
- Ning, M., Li, M., Su, J., Salah, A.A., Ertugrul, I.O., 2024. Elucidating the exposure bias in diffusion models. URL: <https://arxiv.org/abs/2308.15321>, arXiv:2308.15321.
- Ning, M., Sangineto, E., Porrello, A., Calderara, S., Cucchiara, R., 2023. Input perturbation reduces exposure bias in diffusion models, in: *International Conference on Machine Learning*, PMLR. pp. 26245–26265.
- O’Boyle, N.M., Banck, M., James, C.A., Morley, C., Vandermeersch, T., Hutchison, G.R., 2011. Open babel: An open chemical toolbox. *Journal of cheminformatics* 3, 1–14.
- Peng, X., Luo, S., Guan, J., Xie, Q., Peng, J., Ma, J., 2022. Pocket2mol: Efficient molecular sampling based on 3d protein pockets, in: *International Conference on Machine Learning*, PMLR. pp. 17644–17655.
- Ragoza, M., Masuda, T., Koes, D.R., 2022a. Generating 3d molecules conditional on receptor binding sites with deep generative models. *Chemical science* 13, 2701–2713.
- Ragoza, M., Masuda, T., Koes, D.R., 2022b. Generating 3d molecules conditional on receptor binding sites with deep generative models. *Chemical science* 13, 2701–2713.
- Rasul, K., Seward, C., Schuster, I., Vollgraf, R., 2021. Autoregressive denoising diffusion models for multivariate probabilistic time series forecasting, in: *International Conference on Machine Learning*, PMLR. pp. 8857–8868.
- Rognan, D., 2007. Chemogenomic approaches to rational drug design. *British journal of pharmacology* 152, 38–52.
- Satorras, V.G., Hoogeboom, E., Welling, M., 2021. E (n) equivariant graph neural networks, in: *International conference on machine learning*, PMLR. pp. 9323–9332.

- Schoenmaker, L., Béquignon, O.J., Jespers, W., van Westen, G.J., 2023. Uncorrupt smiles: a novel approach to de novo design. *Journal of Cheminformatics* 15, 22.
- Sneider, W., 2005. *Drug discovery: a history*. John Wiley & Sons.
- Sohl-Dickstein, J., Weiss, E., Maheswaranathan, N., Ganguli, S., 2015. Deep unsupervised learning using nonequilibrium thermodynamics, in: *International conference on machine learning*, PMLR. pp. 2256–2265.
- Song, Y., Ermon, S., 2019. Generative modeling by estimating gradients of the data distribution. *Advances in neural information processing systems* 32.
- Song, Y., Sohl-Dickstein, J., Kingma, D.P., Kumar, A., Ermon, S., Poole, B., 2021. Score-based generative modeling through stochastic differential equations, in: *International Conference on Learning Representations*. URL: <https://openreview.net/forum?id=PXTIG12RRHS>.
- Walters, W.P., Barzilay, R., 2020. Applications of deep learning in molecule generation and molecular property prediction. *Accounts of chemical research* 54, 263–270.
- Weininger, D., 1988. Smiles, a chemical language and information system. 1. introduction to methodology and encoding rules. *Journal of chemical information and computer sciences* 28, 31–36.
- White, N., 1997. Assessment of the pharmacodynamic properties of antimalarial drugs in vivo. *Antimicrobial agents and chemotherapy* 41, 1413–1422.
- Xu, M., Yu, L., Song, Y., Shi, C., Ermon, S., Tang, J., 2021. Geodiff: A geometric diffusion model for molecular conformation generation, in: *International Conference on Learning Representations*.
- Yang, L., Cui, Y., Xuan, Y., Wang, C., Belongie, S., Estrin, D., 2018. Unbiased offline recommender evaluation for missing-not-at-random implicit feedback, in: *Proceedings of the 12th ACM conference on recommender systems*, pp. 279–287.
- Zhang, W., Feng, Y., Meng, F., You, D., Liu, Q., 2019. Bridging the gap between training and inference for neural machine translation, in: Korhonen, A., Traum, D., Màrquez, L. (Eds.), *Proceedings of the 57th Annual Meeting of the Association for Computational Linguistics*, Association for Computational Linguistics, Florence, Italy. pp. 4334–4343. URL: <https://aclanthology.org/P19-1426>, doi:10.18653/v1/P19-1426.

Appendix for "Bridging the Gap between Learning and Inference for Diffusion-Based Molecule Generation"

A. Gaussian Posterior of Classic Diffusion Models

We include the Gaussian posterior provided by DDPM for completeness. The classic diffusion model training contains two processes: the forward process and the reverse process. We briefly introduce the main forward formula in equation 2 and the reverse formula in equation 3 in the classic diffusion process. Applying Bayes theorem, we repeat the derivation for the Gaussian posterior here.

$$q(x_{t-1}|x_t, x_0) = \frac{q(x_t|x_{t-1}, x_0)q(x_{t-1}|x_0)}{q(x_t|x_0)} = \frac{q(x_t|x_{t-1})q(x_{t-1}|x_0)}{q(x_t|x_0)} \quad (1)$$

Due to the Markov property of the forward process, x_t is only related to x_{t-1} and not to x_0 . Therefore, we can remove the conditional x_0 from the first term to obtain $q(x_t|x_{t-1})$. Since all three terms in equation 1 are Gaussian distributions and we know the product and the quotient of Gaussian Densities are both Gaussians, the posterior $q(x_{t-1}|x_t, x_0)$ can be written as $\mathcal{N}(x_{t-1}; \tilde{\mu}(x_t, x_0), \tilde{\beta}\mathbf{I})$ (equation 4). The value of mean $\tilde{\mu}_t(x_t, x_0)$ and variance $\tilde{\beta}_t$ are as follows.

$$\tilde{\mu}_t(x_t, x_0) = \frac{\sqrt{\bar{\alpha}_t}\beta_t}{1 - \bar{\alpha}_t}x_0 + \frac{\sqrt{\bar{\alpha}_t}(1 - \bar{\alpha}_{t-1})}{1 - \bar{\alpha}_t}, \quad \tilde{\beta}_t = \frac{1 - \bar{\alpha}_{t-1}}{1 - \bar{\alpha}_t}\beta_t \quad (2)$$

B. The Diffusion Models in Molecule Generation

Due to relevance, we only present the forward process of the diffusion model used for molecular generation tasks in the main text's methodology section. Here, we supplement and explain the reverse process of the diffusion model. Following the classic reverse process, we obtain the main formula $q(M_{t-1}|M_t, M_0, \mathcal{P})$.

$$q(M_{t-1}|M_t, M_0, \mathcal{P}) \quad (3)$$

$$= \frac{q(M_t|M_{t-1}, \mathcal{P})q(M_{t-1}|M_0, \mathcal{P})}{q(M_t|M_0, \mathcal{P})} \quad (4)$$

$$= \frac{P(x_t|x_{t-1}, \mathcal{P})P(v_t|v_{t-1}, \mathcal{P}) \cdot P(x_{t-1}|x_0, \mathcal{P})P(v_{t-1}|v_0, \mathcal{P})}{P(x_t|x_0, \mathcal{P}) \cdot P(v_t|v_0, \mathcal{P})} \quad (5)$$

$$= \frac{P(x_t|x_{t-1}, \mathcal{P})P(x_{t-1}|x_0, \mathcal{P})}{P(x_t|x_0, \mathcal{P})} \quad (6)$$

$$\cdot \frac{P(v_t|v_{t-1}, \mathcal{P})P(v_{t-1}|v_0, \mathcal{P})}{P(v_t|v_0, \mathcal{P})} \quad (7)$$

$$= q(x_{t-1}|x_t, x_0, \mathcal{P}) \cdot q(v_{t-1}|v_t, v_0, \mathcal{P}) \quad (8)$$

After applying Bayes theorem, we can represent the unknown posterior distribution with the known distribution, obtaining the familiar denoising distribution regarding x and v , which can be expressed using $q(x_{t-1}|x_t, x_0, \mathcal{P})$ and $q(v_{t-1}|v_t, v_0, \mathcal{P})$. Utilizing the properties of Gaussian and categorical distributions, we can formulate them into equations 9 and 10 with the same distributions as follows.

$$q(x_{t-1}|x_t, x_0, \mathcal{P}) = \mathcal{N}(x_{t-1}; \tilde{\mu}(x_t, x_0), \tilde{\beta}\mathbf{I}|\mathcal{P}) \quad (9)$$

$$q(v_{t-1}|v_t, v_0, \mathcal{P}) = \mathcal{C}(v_{t-1}|\tilde{c}_t(v_t, v_0), \mathcal{P}) \quad (10)$$

Then, we can compute $\tilde{c}_t(v_t, v_0) = c^* / \sum_{k=1}^K c_k^*$ and $c^*(v_t, v_0)$ while the mean $\tilde{\mu}_t(x_t, x_0)$ and variance $\tilde{\beta}_t$ of positions x are the same as the classic diffusion models.

$$c^*(v_t, v_0) = q(v_t|v_{t-1})q(v_{t-1}|v_0) \quad (11)$$

$$= [\alpha_t v_t + (1 - \alpha_t)/K] \odot [\bar{\alpha}_{t-1} v_0 + (1 - \bar{\alpha}_{t-1})/K] \quad (12)$$